View metadata, citation and similar papers at core.ac.uk

brought to you by CORE

provided by Open Archive Toulouse Archive Ouverte

Open Archive TOULOUSE Archive Ouverte (OATAO)

OATAO is an open access repository that collects the work of Toulouse researchers and makes it freely available over the web where possible.

This is an author-deposited version published in : http://oatao.univ-toulouse.fr/
Eprints ID : 5953

To link to this article : DOI:10.1016/j.electacta.2011.10.101
URL : http://dx.doi.org/10.1016/j.electacta.2011.10.101

To cite this version : Hezard, Teddy and Fajerwerg, Katia and Evrard, David and Colliere, Vincent and Behra, Philippe and Gros, Pierre *Influence of the gold nanoparticles electrodeposition method on Hg(II) trace electrochemical detection.* (2012) Electrochimica Acta, vol. 73. pp. 15-22. ISSN 0013-4686

Any correspondence concerning this service should be sent to the repository administrator: staff-oatao@listes.diff.inp-toulouse.fr

Influence of the gold nanoparticles electrodeposition method on Hg(II) trace electrochemical detection

Teddy Hezard[a,b,c,d], Katia Fajerwerg[e,f,*], David Evrard[c,**], Vincent Collière[e,f], Philippe Behra[a,b], Pierre Gros[c]

[a] Université de Toulouse; INPT, LCA (Laboratoire de Chimie Agro-industrielle); UMR 1010, ENSIACET, 4 allée Emile Monso, F-31030 Toulouse Cedex 4, France
[b] INRA; LCA (Laboratoire de Chimie Agro-industrielle), F-31030 Toulouse, France
[c] Université de Toulouse, Laboratoire de Génie Chimique, UMR CNRS/INPT/UPS 5503, Université Paul Sabatier, F-31062 Toulouse Cedex 9, France
[d] FCS RTRA "Sciences et Technologies pour l'Aéronautique et l'Espace", 23 avenue Edouard Belin, F-31400 Toulouse, France
[e] CNRS, LCC (Laboratoire de Chimie de Coordination), 205 route de Narbonne, F-31077 Toulouse, France
[f] Université de Toulouse, UPS, INPT; LCC, F-31077 Toulouse, France

A B S T R A C T

Gold nanoparticles (AuNPs) were deposited on Glassy Carbon (GC) substrate by using three electrochemical techniques: Cyclic Voltammetry (CV), Chronoamperometry (CA) and Potentiostatic Double-Pulse (PDP). For each electrodeposition method, the resulting AuNPs-modified electrodes were characterized by CV in H_2SO_4 and Field Emission Gun Scanning Electron Microscopy (FEG-SEM). CA was found to be the best electrodeposition mode for controlling the morphology and the density of AuNPs. The modified electrodes were used for low Hg(II) concentration detection using Square Wave Anodic Stripping Voltammetry (SWASV). AuNPs obtained by CA afforded the best amperometric response while involving the lowest amount of charge during the electrodeposition step ($Q_{Au(III)}$). This analytical response is correlated to both the smallest particle size (*ca.* 17 nm in diameter) and the highest particle density (332 particles μm^{-2}), thus displaying high electrode effective surface area. In these optimal conditions, using a Hg(II) preconcentration time of 300 s, the nanosensor array exhibited a linearity range from 0.80 to 9.9 nM with a sensitivity of 1.16 $\mu A\,nM^{-1}$. A detection limit of 0.40 nM (s/n = 3) was reached.

Keywords:
Gold nanoparticles
Electrodeposition mode comparison
Modified electrode characterization
Hg(II) trace determination
Anodic stripping detection

1. Introduction

Since the middle of the 20th century, mercury (Hg) pollution has emerged as a major problem because of its high toxicity. Like most other pollutants (chromium, lead, cadmium, arsenic, pesticides, etc.) the presence of Hg in natural systems causes significant human health problems and environmental risks [1,2]. Among inorganic and organic Hg species, methylmercury and neutral Hg(II) complex species appear to be among the most toxic forms mainly due to their hydrophobic properties and their strong affinity for biological compounds throughout sulphydryl groups [3,4] and DNA binding [5]. Mono and dimethylmercury accumulate in vital organs and tissues [6] and are responsible for many severe diseases such as kidney injury, respiratory failure, central nervous system disorders, brain damages, and can even finally induce death [7]. Moreover, due to bioaccumulation and bioamplification, Hg(II) is highly dangerous even at very low concentration [8–10]. This is consistent with the guideline value of 1 $\mu g\,L^{-1}$ (*ca.* 5 nM) delivered by the World Health Organization and applied in many countries [11]. Thus, Hg(II) trace detection and quantification in the environment is a very challenging research field, and there is an increasing need for analytical systems that deliver fast and reliable data. Particularly, efforts have to be focused on sensitivity enhancements and on the lowering of the detection limits of total Hg.

Leopold et al. recently reviewed the numerous works on spectroscopic techniques that have been reported in the literature with respect to Hg(II) trace analysis [12]. These latter offer selectivity and quite good sensitivity [13], the most common being Cold Vapour Atomic Absorption Spectroscopy (CVAAS) and Cold Vapour Atomic Fluorescence Spectroscopy (CVAFS). Cold vapour generation system can also be coupled to Inductively Coupled Plasma Mass Spectrometry (ICP-MS) and even to multicollector ICP-MS for looking at Hg isotope behaviour in natural system in order to better know its cycling and sources [14]. The double-spike isotope dilution (DSID) methodology also affords accurate and precise results

* Corresponding author at: CNRS, LCC (Laboratoire de Chimie de Coordination), 205 route de Narbonne, F-31077 Toulouse, France. Tel.: +33 05 61 33 31 30; fax: +33 05 61 55 30 03.
** Corresponding author. Laboratoire de Génie Chimique, UMR CNRS/INPT/UPS 5503, Université Paul Sabatier, F-31062 Toulouse Cedex 9, France. Tel.: +33 05 61 55 60 73; fax: +33 05 61 55 61 39.
E-mail addresses: Katia.Fajerwerg@lcc-toulouse.fr (K. Fajerwerg), evrard@chimie.ups-tlse.fr (D. Evrard).

for Hg speciation [15,16]. Although these techniques allow very low concentrations down to 1 pg L^{-1} (*ca.* 5 fM) to be reached, they involve relatively expensive material, specially for ICP-MS method, and require complicated and/or heavy procedures, thus limiting any *in situ* or on line and *operando* analysis.

Comparatively, electrochemical sensing devices represent an interesting alternative. The advantages of the electroanalytical techniques over other detection methods are manifold: low cost, ease of use, low energy requirements and simple procedures, and the possibility to build portable systems that are suitable either for laboratory or on-site measurements. Most of the time, detection limits in the picomolar range can be reached [17,18] by combining a preconcentration step like Anodic Stripping Voltammetry (ASV) [19] and pulsed techniques such as Differential Pulse Voltammetry (DPV) [17,20] or Square Wave Voltammetry (SWV) [18,21,22]. Up to now, many working electrode materials have been used, such as platinum [23], carbon in almost all its forms [20,24–28] and gold (Au). However, because of its strong affinity for Hg that enhances the preconcentration effect during the accumulation step, Au is the most commonly used electrode material. A rapid glance to the literature offers a good insight of the wide range of such systems that have been reported: Au can be used as a bulk [17,21], film [29,30], microwire [18,31], microdisk [32], or microdisk array electrode [33]. Another strategy that is frequently encountered to improve the performances of the electrochemical sensor is the use of chemically modified electrode. The electroactive surface is then functionalized using either polymers [34,35], organic [36] or biological compounds [37,38] chosen for their complexing affinity towards Hg(II).

The development of nanoscale materials in recent years has been extensive, particularly with respect to metallic nanoparticles. Interests have focused on their use in analytical chemistry because of their specific physicochemical properties [39]. These include enhanced diffusion of electroactive species based on high effective surface area of Au nanoparticles (AuNPs), improved selectivity, catalytic activity, higher signal-to-noise ratio and unique optical properties [40]. These attractive properties combined to the strong affinity of Au for Hg favoured the appearance of a new kind of electrode modification involving AuNPs [40,41]. AuNPs can be prepared by chemical synthesis [42,43] or directly by means of electrochemical techniques [44–46]. With respect to Hg(II) trace determination, very few works have been reported till now: AuNPs were electrodeposited by Chronoamperometry (CA) either on Au [47] or Glassy Carbon (GC) [48]. On the other hand, Gong et al. [49] proposed a more complicated system made of bimetallic Au-Pt nanoparticles deposited onto organic nanofibers using Cyclic Voltammetry (CV). Very recently, we reported monometallic AuNPs-modified GC electrode (AuNPs-GC) devoted to low Hg(II) concentration determination [50]. In this latter work, AuNPs have been electrodeposited by CV starting from $HAuCl_4$ and characterized as a function of the charge consumed during the Au(III) reduction step. The AuNPs-GC electrodes allowed a limit of detection of 0.42 nM to be reached, and their analytical performances proved to be strongly correlated to both the density and size of the NPs. The best responses towards Hg(II) trace determination have been recorded for AuNPs-GC electrodes with high density of rather small, spherical-shaped NPs. From these previous results, it has been evidenced that several factors including the control of the electrodeposition conditions are of great importance. In order to study more extensively this aspect, the influence of the electrodeposition method on the analytical performances of AuNPs-GC electrodes has to be considered.

In the present work, we describe the comparison of three different electrodeposition methods, namely CV, CA and Potentiostatic Double-Pulse (PDP). The different AuNPs deposits were characterized by CV in H_2SO_4 and Field Emission Gun Scanning Electron Microscopy (FEG-SEM). For each electrodeposition mode, the analytical performances of the resulting AuNPs-GC electrodes are discussed with respect to the assay of low Hg(II) concentration.

2. Experimental

2.1. Chemicals and apparatus

All the solutions were prepared using ultra pure water (Milli-Q, Millipore, 18.2 MΩ cm). $HAuCl_4 \cdot 3H_2O$ (pro analysis grade) was purchased from Acros Organics. $NaNO_3$ and HCl 30% (suprapur grade) were obtained from Merck. H_2SO_4 95% (normapur grade) was supplied by VWR Prolabo. A standard stock solution of 4.99 ± 0.01 μM Hg(II) was prepared by dilution of 1001 ± 2 mg L^{-1} $Hg(NO_3)_2$ NIST standard solution (certiPUR grade, Merck) and acidified to pH 2 with concentrated HNO_3 65% (suprapur grade, Merck), and then used as it for further dilution.

All the electrochemical experiments were performed at room temperature in a Teflon PFA three-electrode cell (Metrohm) by using a PGSTAT 128 N potentiostat (Metrohm Autolab, Utrecht, Netherlands) interfaced to a laptop computer and controlled with NOVA 1.7 software package (Metrohm). A Metrohm Ag/AgCl/KCl 3 M electrode, separated from the electrochemical cell by a Teflon PTFE capillary containing a 0.1 M $NaNO_3$ solution and terminated by a ceramic diaphragm (D type), and a Metrohm GC wire were used as reference and counter electrodes, respectively. Working electrodes were GC rotating disk electrodes from Radiometer (3 mm diameter, $A = 7.07$ mm^2) or AuNPs-GC. The electrochemical cell was maintained in a Faraday cage in order to minimize the electrical interferences. When indicated, the solutions were deaerated using a N_2 stream for 10 min. A N_2 atmosphere was then maintained over the solution during the corresponding experiments.

2.2. Electrode preparation and modification

Prior to each modification, the GC surfaces were carefully polished successively by silicon carbide grinding paper (grit 1200) for 5 s, and by a 9 μm, 5 μm and 1 μm alumina slurry (Presi) on a cloth polishing pad for 10 min, 5 min and 3 min, respectively. Between each polishing step, the surfaces were cleaned in an ultrasonic ethanol bath (5 min) in order to remove any impurity. Finally, they were rinsed in an ultrasonic ultra pure water bath (5 min) and dried for 1 min using a N_2 stream. Then, the quality of the polishing step was verified by checking the surface state using a Nikon Eclipse LV150 optical microscope.

AuNPs were deposited onto GC electrodes using CV, CA or PDP method and starting from a deaerated 0.1 M $NaNO_3$ solution containing 0.25 mM $HAuCl_4$ (pH 3). The procedure using CV has been previously reported [50]. Briefly, AuNPs were obtained by scanning the working electrode from the open-circuit potential (*ca.* 0.90 V) to 0.00 V at a scan rate of 50 mV s^{-1} for a given number of scans (N).

Electrodeposition using CA was performed at $E_d = 0.00$ V for a given time t_d from 1 to 600 s. For the sake of clarity, the abbreviation CA was used although this method is referring to a constant potential electrolysis.

Concerning PDP, the following conditions were applied for the first pulse: $E_1 = 0.00$ V, $t_1 = 50$ ms; and for the second pulse: $E_d = 0.75$ V, t_d from 1 to 600 s.

Whatever the electrodeposition method used, the resulting electrodes were activated in a 0.5 M H_2SO_4 solution by running 10 scans between 0.20 and 1.40 V at a scan rate of 100 mV s^{-1}.

2.3. AuNPs characterization

The AuNPs-GC surface was characterized by FEG-SEM using a JEOL JSM 6700F equipment with accelerating voltages of 5 and 10 kV and a working distance between 6 and 15 mm depending

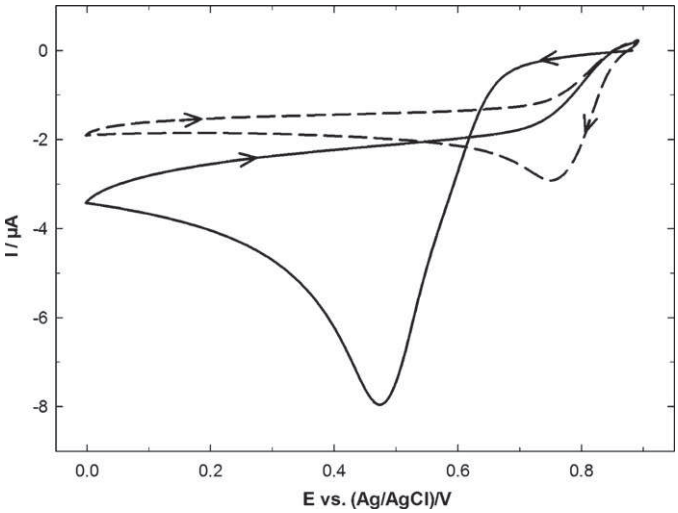

Fig. 1. CVs recorded during Au(III) reduction (according to Reaction (1)) at a GC electrode in a deaerated 0.1 M $NaNO_3$ solution containing 0.25 mM $HAuCl_4$: first (solid line) and second (dashed line) scans (scan rate: 50 mV s^{-1}).

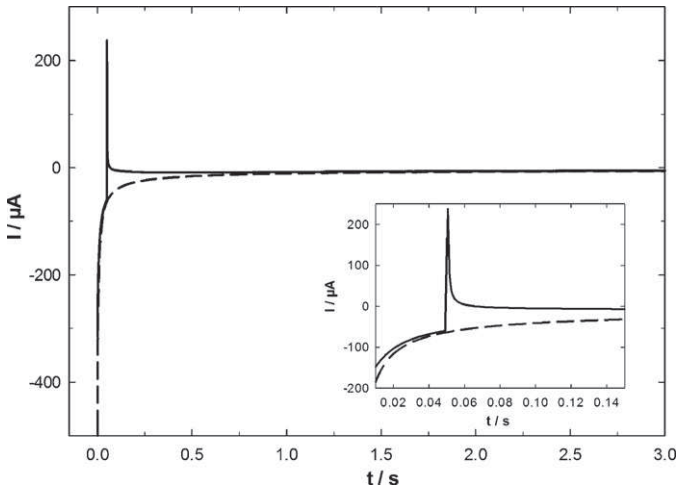

Fig. 2. Current transients recorded at a GC electrode from a deaerated 0.1 M $NaNO_3$ solution containing 0.25 mM $HAuCl_4$: using CA with E_d = 0.00 V for t_d = 3 s (dashed line); using PDP with E_1 = 0.00 V, t_1 = 50 ms and E_d = 0.75 V, t_d = 3 s (solid line).

on the sample. Image analysis was carried out using a homemade program for particles counting (density estimation) and average diameter measurement developed using MATLAB image processing toolbox software. The density and average size of AuNPs was evaluated from a 12.1 μm^2 GC surface analysis, counting a minimum of 390–4000 particles (depending on the charge used during the electrodeposition step $Q_{Au(III)}$). For each deposit, the error was calculated from the analysis of at least three different SEM images. For PDP images, only spherical-shaped NPs were considered for density and size measurements.

2.4. Stripping voltammetric detection of Hg(II)

Electrochemical detection and assay of Hg(II) on AuNPs-GC electrodes were performed in a deaerated (N_2) 0.01 M HCl solution by using Square Wave Anodic Stripping Voltammetry (SWASV) in the following conditions: cleaning potential = 0.80 V, cleaning time = 15 s; preconcentration cathodic potential = 0.00 V, preconcentration time = 300 s; pulse amplitude = 25 mV, step amplitude = 5 mV, frequency = 200 Hz; anodic scan from 0.00 to 0.80 V. During the preconcentration step, the solution was stirred by means of the rotating working electrode (2000 rpm). A second scan was recorded immediately after the first one using the same conditions except the preconcentration time which was set to 30 s, and considered as a blank. Hg(0) reoxidation peak heights (ΔI_p) were measured from the curves obtained after subtraction of the blank. This procedure, called "subtractive ASV method", has been previously reported in the literature [17]. It allows the analytical results to be released from background vagaries (see Section 3 for further precisions). It is noteworthy that the subtractive anodic signals recorded with low Hg(II) concentrations were noisy so we needed to use a Savitzky–Golay smoothing function.

3. Results and discussion

3.1. AuNPs electrodeposition on GC electrode

Fig. 1 shows the first two scans obtained by CV on GC with a 0.25 mM $HAuCl_4$ solution. The forward scan (Fig. 1, solid line) of the voltammogram exhibits the reduction of Au(III) to Au(0) with a cathodic peak at 0.48 V, inducing the deposition of AuNPs onto the electrode surface according to Reaction (1):

$$AuCl_4^- + 3e^- \rightarrow Au + 4Cl^- \quad (1)$$

On the backward scan, a current crossover occurred at 0.62 V: beyond this point, the backward cathodic current became higher than the forward one. This is consistent with thermodynamics which predicts an easier growth of previously formed AuNPs than a nucleation of new AuNPs on GC electrode. On the second scan (Fig. 1, dashed line) the Au(III) reduction peak shifted to a less cathodic potential (*ca.* 0.78 V), indicating that in the potential range between 0.48 and 0.78 V Au(0) deposition occurred more easily on the NPs created during the first scan.

From this voltammogram, a potential of E_d = 0.00 V was chosen as the working potential for electrodeposition experiments using CA. Such a value corresponds to an overpotential $\eta_1 = -0.70$ V large enough to favour the establishment of new nucleation sites over the growth of previously created nuclei [51,52]. The electrodeposition time t_d was varied from 1 to 600 s. Whatever the t_d value used, the current transients all exhibited a typical shape which has been previously reported by El-Deab [53] and Komsiyska and Staikov [52] (Fig. 2, dashed line): first, an initial high cathodic current due to the charging of the double-layer; initial nuclei are formed at this early stage. Then, a current decay which follows Cottrell's law (proportional to $t^{-1/2}$), and corresponds to a planar diffusion regime arising from the overlapping of the growing hemispherical diffusion layers in the neighbouring of the NPs [45]. In all this series of experiments the overpotential used was high enough so that the "hump-shaped" response following the charging current spike described by Finot et al. [51] was not observed.

Fig. 2 (solid line) presents the current transient obtained using PDP for the electrodeposition method. At short time values ($0 < t < t_1$), this curve exhibits the same shape than the CA one corresponding to the charging of the double-layer and the formation of the first nuclei. When switching from E_1 = 0.00 to E_d = 0.75 V (PDP), a break was observed on the current transient (Fig. 2, inset) and an anodic current was recorded for a short time. This positive current may be explained as the result of a destabilization of the NPs due to overlapping diffusion zones. When switching from E_1 to E_d, only the largest nuclei formed during the first pulse are stable under the second pulse and NPs whose radii r are lower than $r_{critical}$ dissolve [54,55]. Then the current transient became negative again and the increase in the cathodic current observed between 0.06 and 0.36 s is associated to the growth process of NPs. Finally, at longer time

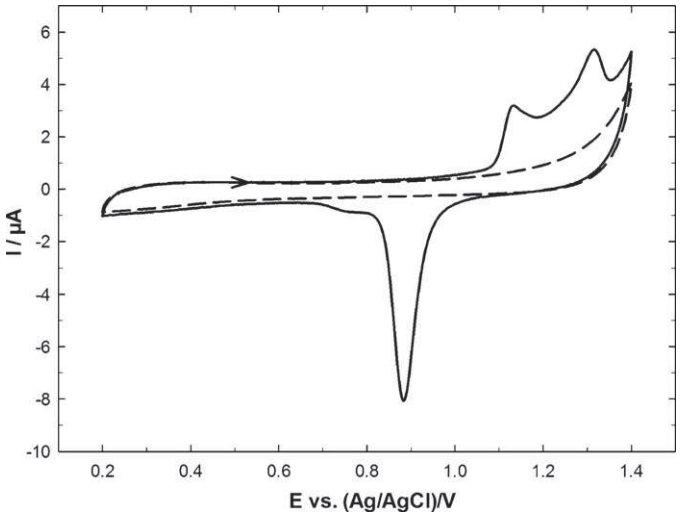

Fig. 3. CVs recorded in a 0.5 M H_2SO_4 solution on a AuNPs-GC electrode prepared by CA using t_d = 15 s (solid line) and on an unmodified GC electrode (dashed line) (scan rate: 100 mV s^{-1}).

the current transient decreased again following Cottrell's law in the same way than the CA curve.

3.2. Characterization of AuNPs-GC

3.2.1. Electrochemical characterization

AuNPs deposits were characterized by performing CV experiments in a 0.5 M H_2SO_4 solution, scanning the potential between 0.20 and 1.40 V. Fig. 3 provides an example for AuNPs electrodeposited by CA using t_d = 15 s (solid line). The voltammograms exhibited the well-known anodic peaks between 1.10 and 1.35 V which correspond to the formation of different kinds of Au oxides [56], mainly AuO according to Reaction (2):

$$Au + H_2O \rightarrow AuO + 2H^+ + 2e^- \quad (2)$$

On the backward scan a reduction peak at 0.87 V was observed which was associated to the subsequent reduction of the oxides formed during the forward scan. Comparatively a small residual current was recorded in the same experimental conditions using an unmodified GC electrode (Fig. 3, dashed line). Whatever the electrodeposition method used, the shape of voltammograms was found to be similar for a given electrodeposition charge $Q_{Au(III)}$ used. Increasing this charge, the shape of the anodic part of voltammograms slightly evolved, according to a variation of the relative ratios of the different crystallographic faces of AuNPs [53,57]. Table 1 summarizes the values of the charge corresponding to the electrodeposition step $Q_{Au(III)}$ using either CA, PDP or CV, and the charge related to Au oxides reduction Q_{oxides} obtained from Fig. 3. On one hand, $Q_{Au(III)}$ recorded for CA is in the same order of magnitude than that obtained using PDP whatever the Au electrodeposition time. This result is in accordance with Fig. 2 where the current transients are the same for both electrochemical methods. It is not surprising if it is considered that the amount of charge consumed for the nuclei formation is negligible compared to the one necessary for the NPs growth in the deposition time range studied. The mean difference is logically obtained for the shorter total electrolysis time, corresponding to the highest ratio $t_1/(t_1 + t_d)$ in PDP mode. On the other hand the amount of charge Q_{oxides} is strongly lower than $Q_{Au(III)}$. Assuming that 3 electrons are exchanged during Au(III) reduction and 2 for Au oxides formation (according to Reaction (2)) and that the faradic yield for Au electrodeposition is 100%, and considering that Q_{oxides} is equal to the amount of Au which is oxidized during the CVs in H_2SO_4, this latter is calculated from the following relation: $n_{AuO}/n_{Au} = 1.5 \times Q_{oxides}/Q_{Au(III)}$. In the case of PDP, this ratio decreases from about 17 to 3.6% when increasing the electrodeposition time. Consequently only the Au atom layers at the AuNPs-electrolyte interface are believed to be effectively oxidized, this part decreasing with increasing particles size.

3.2.2. Density and size characterization

In order to further characterize the deposits, SEM-FEG analyses were performed. Fig. 4 shows typical images obtained using CA (frames A–D), PDP (frames E–H) and CV (frames I–L) for different electrodeposition conditions. The NPs density and size are also summarized in Table 1. The deposits obtained by CA were homogeneous with small and nearly hemispherical-shaped AuNPs for deposition times t_d lower than 300 s. The overpotential $\eta_1 = -0.70$ V was large enough to achieve instantaneous nucleation and then effectively seed the surface with nuclei at short t_d. This is consistent with the fact that the density reached an optimum, *i.e.* 332 NPs/µm^2 (Table 1, entry 3). At the same time, the average size increased with the deposition time and then $Q_{Au(III)}$. For t_d = 300 s (frame C) faceted and some polyhedral AuNPs started to appear and at t_d = 600 s Au "popcorn-like" nanoclusters were formed (frame D). This morphology could result from a simultaneous aggregation of AuNPs already present on the surface and the formation of new nuclei.

Many studies claim that the PDP procedure is an efficient way to control the growth of the nuclei formed during the first pulse E_1 since the short time t_1 associated to this step should favour monodispersity of the deposits [52,55,58–60]. Indeed, the first pulse is used to initiate the formation of nuclei and the second pulse E_d, more positive than E_1 is used to favour their growth [54,58–60]. The AuNPs morphology obtained in this present study using this electrodeposition mode can be divided into two kinds of populations (frames E–H): the first one is related to isotropic and spherical-shaped NPs for $t_d \leq 30$ s and the second one to anisotropic nanowires [61,62]. The presence of these two kinds of populations was even more evident when the deposition time t_d increased beyond 300 s. The insets in Fig. 4 (F and G) are high-magnification SEM-FEG images of the nanowires which illustrate that these latter should result from a coalescence phenomenon. The NPs density (*ca.* 200 NPs/µm^2) was nearly constant in all the t_d range considered (Table 1). This tendency is not surprising while considering that the stable nuclei formed during the first pulse (large overpotential) should be preserved [54].

The evolution of the morphology and the density of AuNPs electrodeposited by CA, PDP and CV [50] depends on the charge for electroreduction steps $Q_{Au(III)}$, *i.e.* low (*ca.* 100 µC) and high (*ca.* 800 µC) whatever the electrodeposition method. Briefly, it can be clearly observed that at low $Q_{Au(III)}$ the density recorded for CA (239 NPs/µm^2, Table 1, entry 4) is in the same order of magnitude than that obtained using PDP (259 NPs/µm^2, Table 1, entry 10). The value obtained in the latter case seems to be slightly overestimated. For the CV method, two distinct populations of electrodeposited AuNPs can be also distinguished (frames I–L). The first population of particles is attributed to small and spherical-shaped NPs and the second one to larger, aggregate-like NPs. In our previous work [50], an increase in the particle density has been noticed up to 4 potential scans, and then the density decreased down to 12 cycles and finally remained nearly constant till 20 scans. This evolution of both the AuNPs density and average size indicates a gradual aggregation and/or coalescence phenomenon up to a critical value more or less pronounced whatever the electrodeposition method used.

3.3. Electrochemical response and optimization towards Hg(II) detection

In order to test and optimize the response of AuNPs-GC electrodes towards low Hg(II) concentration detection, a series of

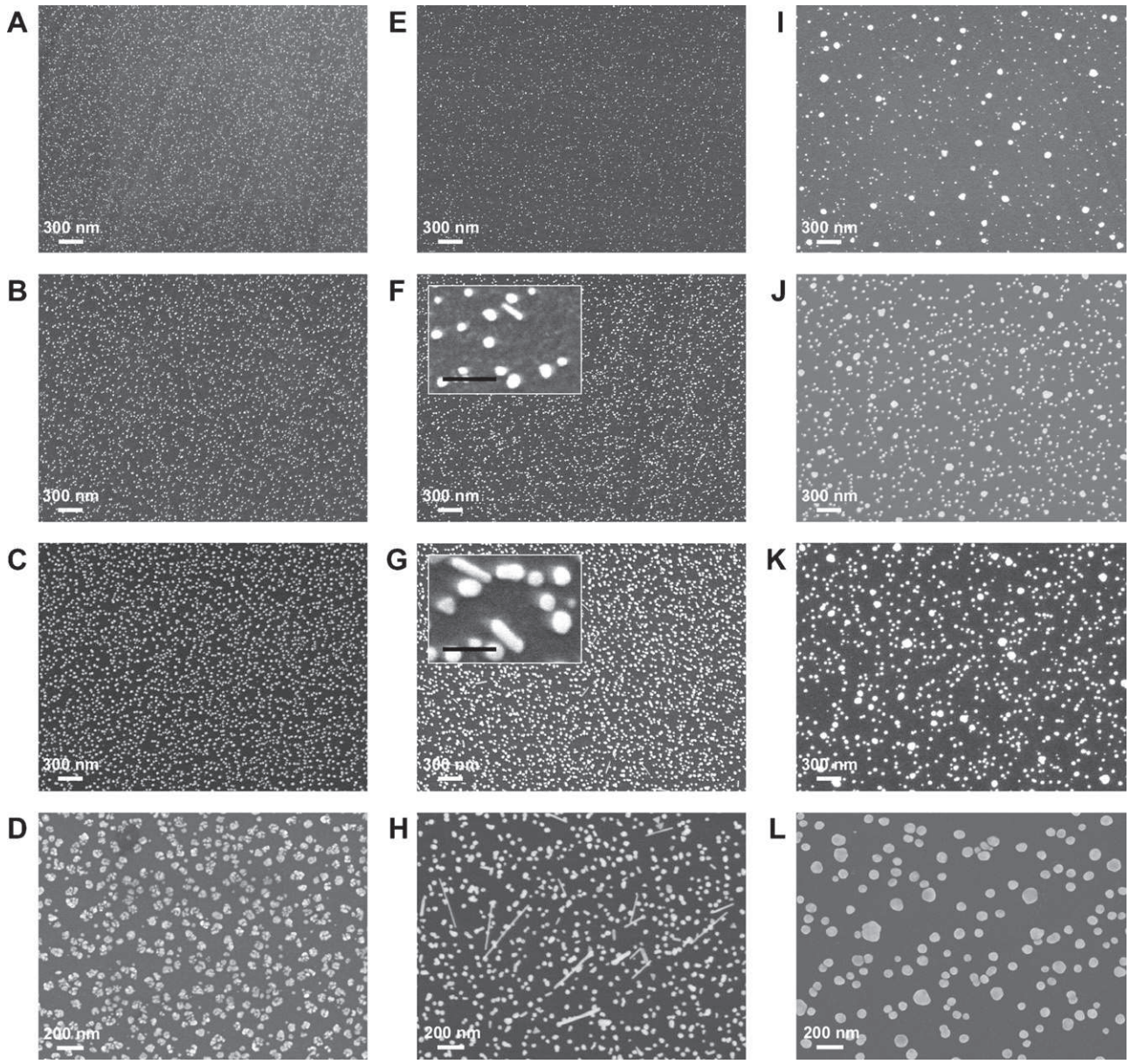

Fig. 4. FEG-SEM images of AuNPs-GC electrodes prepared from a deaerated 0.1 M $NaNO_3$ solution containing 0.25 mM $HAuCl_4$ using CA (A, B, C, D), PDP (E, F, G, H) and CV (I, J, K, L). Conditions for CA: E_d = 0.00 V for t_d = 3 s (A), 30 s (B), 300 s (C) and 600 s (D); Conditions for PDP: E_1 = 0.00 V, t_1 = 50 ms and E_d = 0.75 V for t_d = 3 s (E), 30 s (F), 300 s (G) and 600 s (H); Number of scans for CV: 1 (I), 4 (J), 8 (K) and 20 (L). The scale bars in the insets (F and G) are 100 nm.

experiments was performed with the different deposits obtained by CA and PDP. Fig. 5 shows the typical SWASV recorded for a 4.0 nM Hg(II) concentration in 0.01 M HCl using AuNPs-GC electrode prepared by CA (t_d = 15 s). This concentration was chosen because it is easily detectable and allows further optimization of the system. For a preconcentration time of 300 s (E = 0.00 V), a broad baseline centred at 0.30 V was observed together with a sharp peak at 0.58 V (Fig. 5, solid line) which corresponds to Hg(0) reoxidation according to Reaction (3):

$$Hg + 2Cl^- \rightarrow HgCl_2 + 2e^- \quad (3)$$

Hg(II) was first reduced to Hg(0) during the preconcentration step and then reoxidized at 0.58 V during the stripping step. Contrary to what has been previously reported by several authors [22,48], we recently assumed that the broad baseline was not due to calomel formation but to an oxidation of AuNPs surface in the presence of Cl^- ions [50]. So, as the background depends on the amount of accessible sites of Au atoms, recording a SWASV in the absence of Hg(II) in the solution was not suitable as a blank. In order the peak current at 0.58 V to be used for an analytical purpose, an experiment was thus carried out with a preconcentration time of 30 s (Fig. 5, dashed line). In these conditions, a small shoulder was only observed in the region of Hg(0) reoxidation. This curve was then used as an analytical blank and subtracted to the former one (Fig. 5, inset).

The effect of both the electrodeposition method and the amount of electrodeposited AuNPs ($Q_{Au(III)}$) was then examined using SWASV for a 4.0 nM Hg(II) solution. Fig. 6 shows the variation of the subtractive peak current (ΔI_p) corresponding to Hg(0) reoxidation (blank subtracted) as a function of $Q_{Au(III)}$ for CA and PDP. For both methods, a rapid increase with a maximum in ΔI_p is observed at low $Q_{Au(III)}$ values, *ca.* between 36 and 119 μC (t_d = 3 s and 30 s, respectively) for CA and 110 μC (t_d = 30 s) for PDP. Then, ΔI_p gradually decreased while $Q_{Au(III)}$ increased. This is consistent with our previous finding with CV electrodeposition (Table 1) that the best analytical responses were recorded for a high density of

Table 1
Characterization of AuNPs on GC and ΔI_p of Hg(0) reoxidation for CA and PDP at different deposition times t_d during the electrodeposition step, and for CV using different numbers of scans (N).

Entry	Method	t_d (s)	$Q_{Au(III)}$ (μC)[a]	Q_{oxides} (μC)[b]	NPs density (μm^{-2})[c]	Average diameter (nm)[c]	ΔI_p (μA)[d]
1	CA	1	21	1.9	151 ± 4	15 ± 3 (1830)	5.7 ± 0.8
2		3	36	1.4	326 ± 2	16 ± 4 (3930)	6.7 ± 0.2
3		15	78	4.5	332 ± 5	17 ± 4 (4000)	6.8 ± 0.3
4		30	119	4.7	239 ± 3	20 ± 4 (2885)	6.6 ± 0.2
5		300	496	11.6	220 ± 5	31 ± 7 (2650)	4.6 ± 0.4
6		600	825	23.2	119 ± 9	47 ± 16 (1455)	3.0 ± 0.2
7	PDP	1	15	1.7	199 ± 7	13 ± 3 (2400)	4.0 ± 0.7
8		3	26	2.0	193 ± 3	13 ± 3 (2320)	5.6 ± 0.4
9		15	72	4.2	193 ± 2	19 ± 5 (2325)	5.9 ± 0.1
10		30	110	4.9	259 ± 5	18 ± 5 (3115)	6.7 ± 0.2
11		300	445	12.0	192 ± 5	32 ± 9 (2335)	5.0 ± 0.2
12		600	883	21.4	159 ± 7	34 ± 10 (1915)	3.0 ± 0.1
13	CV	N = 1	99	2.7	53 ± 2	27 ± 16 (635)	5.0 ± 1.3
14		N = 4	260	5.8	73 ± 3	36 ± 13 (860)	7.0 ± 0.4
15		N = 8	437	9.4	64 ± 3	41 ± 15 (805)	6.5 ± 0.2
16		N = 20	846	20	32 ± 2	71 ± 20 (390)	4.3 ± 0.2

[a] $Q_{Au(III)}$ is the charge consumed during the electroreduction step in 0.25 mM $HAuCl_4$.
[b] Q_{oxides} is the charge corresponding to the reduction of Au oxides in 0.5 M H_2SO_4.
[c] See Section 2 for details on NPs density and average diameter estimation. The values in brackets correspond to the average number of NPs considered for the calculation.
[d] ΔI_p is the subtractive peak current of Hg(0) reoxidation measured from a 4.0 nM Hg(II) solution (see Fig. 5).

small NPs as far as the AuNPs deposits may be viewed as an array of spherical-shaped Au "nanoelectrodes" [50]. While increasing t_d for both electrodeposition methods, growth processes are favoured to the detriment of new nuclei formation, thus leading to bigger NPs and probably aggregation and/or coalescence phenomena, respectively. As a consequence, the current decreases due to the decrease in the number of "nanoelectrodes". All these results suggest that the amperometric response of the modified electrode strongly depends on the effective surface area of the AuNPs. The latter increases with the number and the small size of AuNPs (high surface to volume ratio). The effective surface area increases with the number of NPs for the lowest $Q_{Au(III)}$ and decreases for the highest $Q_{Au(III)}$ because of coalescence phenomena. In other words, the highest the total AuNPs effective surface area, the best the performances. However, in the case of CA, the maximum in ΔI_p was observed in a t_d range from 3 s ($Q_{Au(III)}$ = 36 μC) to 30 s ($Q_{Au(III)}$ = 119 μC), suggesting that for low electrodeposition charge values, this method affords more homogeneous deposits than PDP. Moreover, in the optimal t_d range, the density of AuNPs is higher for CA than for PDP. Finally, CA provided similar analytical responses while involving lower $Q_{Au(III)}$. For these reasons, CA was chosen for low Hg(II) concentration assay.

3.4. Analytical performances towards low Hg(II) concentration assay

From the analysis of Fig. 6, an AuNPs-GC electrode prepared by CA using t_d = 15 s (optimal conditions) was chosen to study the response towards low Hg(II) concentration. Successive amounts of Hg(II) were added to a 0.01 M HCl solution, and the corresponding SWASV recorded (Fig. 7). Under the optimized experimental conditions (see SWASV parameters as described in Section 2), the AuNPs-GC electrode exhibited a good linearity in the range 0.80–9.9 nM (7 standard concentrations) with a correlation coefficient of 0.9995 (Fig. 7, inset). From the slope of the calibration plot, the sensitivity of the AuNPs-GC electrode was found to be

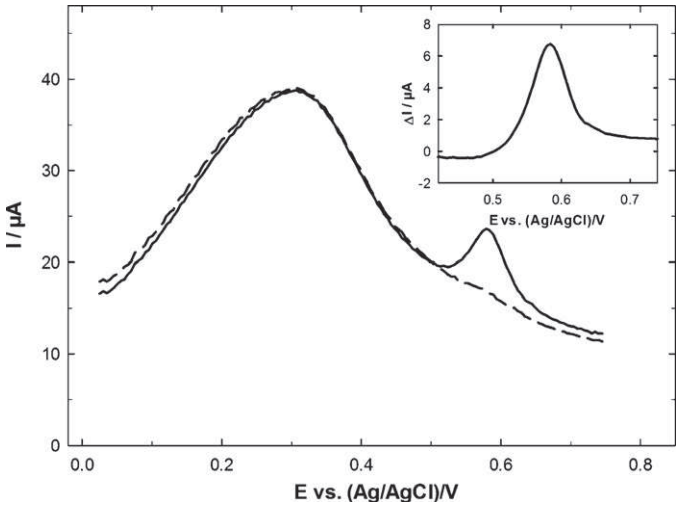

Fig. 5. Typical SWASV signals recorded at a AuNPs-GC electrode prepared by CA (t_d = 15 s, $Q_{Au(III)}$ = 78 μC) in a 0.01 M HCl solution containing 4.0 nM Hg(II) for a preconcentration time of 300 s (solid line) and 30 s (dashed line). Inset: resulting signal after subtraction of dashed line from solid line.

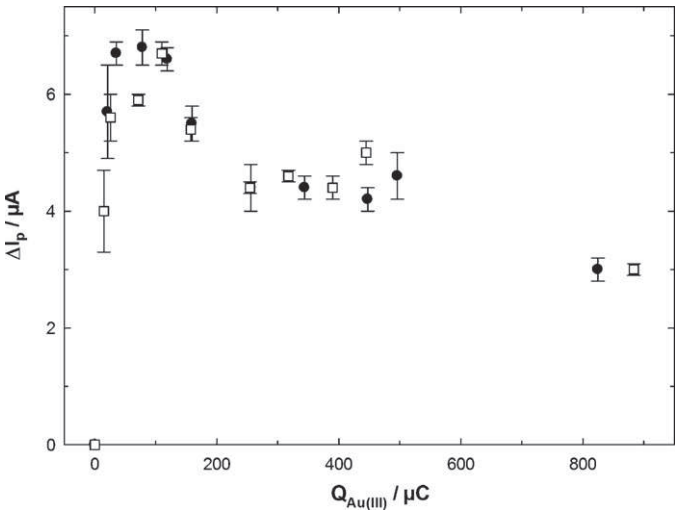

Fig. 6. Variation of the subtractive peak current (ΔI_p) observed by SWASV at E = 0.58 V with a 4.0 nM Hg(II) concentration in 0.01 M HCl as a function of the amount of charge consumed during AuNPs electrodeposition ($Q_{Au(III)}$) using CA with E_d = 0.00 V for t_d = 1–600 s (black-coloured circles) and PDP with E_1 = 0.00 V for t_1 = 50 ms and E_d = 0.75 V for t_d = 1–600 s (white-coloured squares).

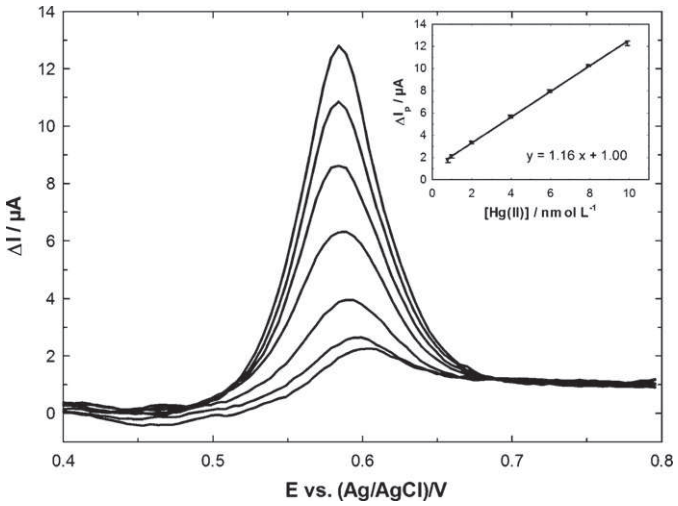

Fig. 7. SWASV responses obtained in a 0.01 M HCl solution for increasing Hg(II) concentrations (blank subtracted) on a AuNPs-GC electrode prepared by CA using t_d = 15 s. From bottom to top: 0.8, 1.0, 2.0, 4.0, 5.9, 7.9 and 9.9 nM Hg(II), respectively. Inset: ΔI_p *vs.* [Hg(II)] and linear regression.

1.16 μA nM^{-1}. A limit of detection (LD) of 0.40 nM was calculated for a signal-to-noise ratio of 3 [63]. This value could be easily improved using longer Hg preconcentration time. These results are consistent with our previous findings dealing with an electrode prepared using CV [50] in which we reported a sensitivity of 1.37 μA nM^{-1} in a concentration range from 0.64 to 4.0 nM, and a LD of 0.42 nM. Both LD and sensitivity exhibit comparable values, the latter one being however slightly better for CV, considering a same value of Hg(II) preconcentration time (300 s). Nevertheless, the linearity range afforded by CA is more than twice wider (upper limit: 9.9 nM for CA, *vs.* 4.0 nM for CV) since a saturation phenomenon begins to occur in the case of CV for Hg(II) concentrations higher than 4 nM, which is not observed here for CA. This suggests that CA allows a better control of the Au deposit, leading to a higher effective surface area than CV for the same amount of charge consumed during the electrodeposition step. Moreover, the optimal conditions for low Hg(II) concentration detection were obtained for $Q_{Au(III)}$ values between two and five times lower for CA (Table 1, entries 2–4) than for CV (Table 1, entry 14).

4. Conclusions

In this work, two different electrodeposition methods of AuNPs, namely CA and PDP, were used for low Hg(II) concentration assay and compared with previous results obtained by CV [50]. The different AuNPs deposits obtained were characterized using CV in H_2SO_4 and FEG-SEM analysis. From the set of results, CA was found to afford the best morphological and density control of the AuNPs. Indeed, more homogeneous deposits with more spherical-shaped NPs for rather short electrodeposition times ($t_d \leq 300$ s) were obtained. CA also provided better analytical responses towards Hg(II) detection than PDP and CV, since comparable ΔI_p were recorded for lower $Q_{Au(III)}$. We thus suggest that the results are strongly correlated to the effective surface area of the AuNPs: the highest the effective surface area, the best the performances. In the optimal conditions, the response of the AuNPs-GC electrode was linear in the range 0.80–9.9 nM with a sensitivity of 1.16 μA nM^{-1}, and a LD of 0.40 nM was obtained. Further work is necessary to optimize analytical parameter by coupling experiments and modelling.

Acknowledgments

This work was part of a project financially supported by the Fondation STAE (Sciences et Technologies pour l'Aéronautique et l'Espace) under the acronym "MAISOE" (Microlaboratoires d'Analyses *In Situ* pour des Observatoires Environnementaux). The authors thank Dr. Yannick Hallez and Dr. Jérémie Viguié for their help in MATLAB programming. The authors thank the referees for their fruitful comments.

References

[1] D.Q. Hung, O. Nekrassova, R.G. Compton, Talanta 64 (2004) 269.
[2] A. Bobrowski, A. Krolicka, J. Zarebski, Electroanalysis 21 (2009) 1449.
[3] M.J. Stillman, D. Thomas, C. Trevithick, X. Guo, M. Siu, J. Inorg. Biochem. 79 (2000) 11.
[4] A. Leiva-Presa, M. Capdevila, P. Gonzalez-Duarte, Eur. J. Biochem. 271 (2004) 4872.
[5] I. Onyido, A.R. Norris, E. Buncel, Chem. Rev. 104 (2004) 5911.
[6] M. Korbas, S.R. Blechinger, P.H. Krone, I.J. Pickering, G.N. George, Proc. Natl. Acad. Sci. U.S.A. 105 (2008) 12108.
[7] G.E. McKeown-Eyssen, J. Ruedy, A. Neims, Am. J. Epidemiol. 118 (1983) 470.
[8] F.M.M. Morel, A.M.L. Kraepiel, M. Amyot, Annu. Rev. Ecol. Syst. 29 (1998) 543.
[9] R. Eisler, Environ. Geochem. Health 25 (2003) 325.
[10] Q. Wang, D. Kim, D.D. Dionysiou, G.A. Sorial, D. Timberlake, Environ. Pollut. 131 (2004) 323.
[11] Guidelines for Drinking-water Quality, 3rd ed., vol. 1: Recommendations, World Health Organization, Geneva. http://www.who.int/water_sanitation_health/dwq/gdwq3rev/en/, 2008 (accessed 16.06.11.).
[12] K. Leopold, M. Foulkes, P. Worsfold, Anal. Chim. Acta 663 (2010) 127.
[13] S.K. Pandey, K.-H. Kim, R.J.C. Brown, Trends Anal. Chem. 30 (2011) 899.
[14] L. Laffont, J.E. Sonke, L. Maurice, H. Hintelmann, M. Pouilly, Y. Sanchez Bacarreza, T. Perez, P. Behra, Environ. Sci. Technol. 43 (2009) 8985.
[15] M. Monperrus, P. Rodriguez Gonzalez, D. Amouroux, J.I. Garcia Alonso, O.F.X. Donard, Anal. Bioanal. Chem. 390 (2008) 655.
[16] L. Laffont, J.E. Sonke, M. Maurice, S. Luna Monrroy, J. Chincheros, D. Amouroux, P. Behra, Environ. Sci. Technol., in press.
[17] L. Sipos, H.W. Nürnberg, P. Valenta, M. Branica, Anal. Chim. Acta 115 (1980) 25.
[18] P. Salaun, C.M.G. van den Berg, Anal. Chem. 78 (2006) 5052.
[19] K.Z. Brainina, N.A. Malakhova, N.Y. Stojko, Fresenius. J. Anal. Chem. 368 (2000) 307.
[20] S. Meyer, F. Scholz, R. Trittler, Fresenius. J. Anal. Chem. 356 (1996) 247.
[21] Y. Bonfil, M. Brand, E. Kirowa-Eisner, Anal. Chim. Acta 424 (2000) 65.
[22] A. Giacomino, O. Abollino, M. Malandrino, E. Mentasti, Talanta 75 (2008) 266.
[23] J.M. Pinilla, L. Hernandez, A.J. Conesa, Anal. Chim. Acta 319 (1996) 25.
[24] D. Jagner, Anal. Chim. Acta 105 (1979) 33.
[25] J. Svarc-Gajic, Z. Stojanovic, Z. Suturovic, N. Marjanovic, S. Kravic, Desalination 249 (2009) 253.
[26] M. Shamsipur, J. Tashkhourian, B. Hemmateenejad, H. Sharghi, Talanta 64 (2004) 590.
[27] H. Yi, Anal. Bioanal. Chem. 377 (2003) 770.
[28] G.G. Muntyanu, J. Anal. Chem. 56 (2001) 546.
[29] E.A. Viltchinskaia, L.L. Zeigman, D.M. Garcia, P.F. Santos, Electroanalysis 9 (1997) 633.
[30] L.A. Khustenko, L.N. Larina, B.F. Nazarov, J. Anal. Chem. 58 (2003) 262.
[31] S. Daniele, C. Bragato, M.A. Baldo, J. Wang, J. Lu, Analyst 125 (2000) 731.
[32] C. Garnier, L. Lesven, G. Billon, A. Magnier, O. Mikkelsen, I. Pizeta, Anal. Bioanal. Chem. 386 (2006) 313.
[33] O. Ordeig, C.E. Banks, J.D. Campo, F.X. Munoz, R.G. Compton, Electroanalysis 18 (2006) 573.
[34] P. Ugo, L. Sperni, L.M. Moretto, Electroanalysis 9 (1997) 1153.
[35] K.-S. Yoo, S.-B. Woo, J.-Y. Jyoung, Bull. Korean Chem. Soc. 24 (2003) 27.
[36] M. Colilla, M.A. Mendiola, J.R. Procopio, M.T. Sevilla, Electroanalysis 17 (2005) 933.
[37] J. Wu, L. Li, B. Shen, G. Cheng, P. He, Y. Fang, Electroanalysis 22 (2010) 479.
[38] D. Wu, Q. Zhang, X. Chu, H. Wang, G. Shen, R. Yu, Biosens. Bioelectron. 25 (2010) 1025.
[39] Y. Liu, G. Su, B. Zhang, G. Jiang, B. Yan, Analyst 136 (2011) 872.
[40] C.M. Welch, R.G. Compton, Anal. Bioanal. Chem. 384 (2006) 601–619.
[41] M. Oyama, Anal. Sci. 26 (2010) 1.
[42] M. Grzelczak, J. Perez-Juste, P. Mulvaney, L.M. Liz-Marzan, Chem. Soc. Rev. 37 (2008) 1783.
[43] Z. Wang, L. Ma, Coord. Chem. Rev. 253 (2009) 1607.
[44] X. Dai, O. Nekrassova, M.E. Hyde, R.G. Compton, Anal. Chem. 76 (2004) 5924.
[45] F.W. Campbell, R.G. Compton, Anal. Bioanal. Chem. 396 (2010) 241.
[46] U.S. Mohanty, J. Appl. Electrochem. 41 (2011) 257.
[47] X.H. Gao, W.Z. Wei, L. Yang, T.J. Yin, Y. Wang, Anal. Lett. 38 (2005) 2327.
[48] O. Abollino, A. Giacomino, M. Malandrino, G. Piscionieri, E. Mentasti, Electroanalysis 20 (2008) 75.
[49] J. Gong, T. Zhou, D. Song, L. Zhang, X. Hu, Anal. Chem. 82 (2010) 567.
[50] T. Hezard, K. Fajerwerg, D. Evrard, V. Collière, P. Behra, P. Gros, J. Electroanal. Chem., in press.

[51] M.O. Finot, G.D. Braybrook, M.T. McDermott, J. Electroanal. Chem. 466 (1999) 234.
[52] L. Komsiyska, G. Staikov, Electrochim. Acta 54 (2008) 168.
[53] M.S. El-Deab, Electrochim. Acta 54 (2009) 3720.
[54] G. Sandmann, H. Dietz, W. Plieth, J. Electroanal. Chem. 491 (2000) 78.
[55] M. Ueda, H. Dietz, A. Anders, H. Kneppe, A. Meixner, W. Plieth, Electrochim. Acta 48 (2002) 377.
[56] H. Angerstein-Kozlowska, B.E. Conway, A. Hamelin, L. Stoicoviciu, Electrochim. Acta 31 (1986) 1051.
[57] A.P. O'Mullane, S.J. Ippolito, Y.M. Sabri, V. Bansal, S.K. Bhargava, Langmuir 25 (2009) 3845.
[58] H. Liu, R.M. Penner, J. Phys. Chem. B 104 (2000) 9131.
[59] H. Liu, F. Favier, K. Ng, M.P. Zach, R.M. Penner, Electrochim. Acta 47 (2001) 671.
[60] E. Sheridan, J. Hjelm, R.J. Forster, J. Electroanal. Chem. 608 (2007) 1.
[61] R.M. Penner, J. Phys. Chem. B 106 (2002) 3339.
[62] L.G. Abdelmoti, F.P. Zamborini, Langmuir 26 (2010) 13511.
[63] Analytical Methods Committee, Analyst 112 (1987) 199.